

ONSAGER'S REAL CAVITY MODEL NEAR SOLID INTERFACES

Johannes Fiedler

Department of Physics and Technology
University of Bergen
Allégaten 55, 5007 Bergen, Norway.
johannes.fiedler@uib.no

Drew F. Parsons

Department of Chemical and Geological Sciences
University of Cagliari
Cittadella Universitaria, 09042 Monserrato, CA, Italy.
drew.parsons@unica.it

ABSTRACT

We develop an extended Onsager real-cavity framework to describe the Casimir–Polder interaction of small molecules dissolved in dielectric liquids near planar interfaces. By analytically resolving the geometry of the cavity opening, we derive a closed expression that arise when the molecule approaches a surface and connect them smoothly to the asymptotic medium-assisted interaction. Using experimentally established dielectric functions for water, propanol, and PTFE together with accurate molecular polarisabilities for O_2 and N_2 , we compute the full distance-dependent potential for four molecule (O_2 and N_2)-liquid (water and propanol)-surface (PTFE) combinations. The results reveal how local-field screening inside the cavity, molecular polarisability, and liquid permittivity jointly determine the magnitude and shape of the interaction, including the characteristic transition from the open cavity (small separations) and closed cavity (large separations). The framework provides a transparent baseline for dispersion forces in liquids, while highlighting limitations associated with the point-dipole description, the absence of repulsive contributions, and the breakdown of the dipole approximation at ultrashort separations.

1 Introduction

Van der Waals forces are fundamental interactions between neutral, polarisable particles [1, 2, 3], crucial for cohesion in materials and for biological adhesion phenomena, such as geckos walking on smooth surfaces [4]. These dispersion forces are increasingly relevant in nanoscale technologies [5, 6, 7, 8, 9, 10, 11] and have been thoroughly studied both experimentally [12, 13, 14, 15] and theoretically [16, 17, 18, 19].

Despite their origin in quantum electrodynamic fluctuations [20], dispersion forces—such as the Casimir [21], Casimir–Polder [16], and London–van der Waals [3] forces—are among the weakest forces in nature. They arise from correlated ground-state fluctuations of the electromagnetic field. While classical approaches often model these forces in vacuum [16, 1, 22], real-world systems such as colloids, proteins, or nanoparticles typically reside in polar media like water or organic solvents [23].

The medium alters the interaction range and sign [24, 25], often invalidating simple vacuum-based asymptotics [26]. The interplay between retardation, thermal fluctuations, and dielectric screening can result in nonmonotonic potentials and even repulsive forces [27, 28, 29]. Such features enable novel trapping mechanisms [30, 31, 32, 33] without the need for external stabilising forces.

While various microscopic models (e.g., molecular dynamics [34, 35, 36, 37]) have been developed to address solvent effects on ion distributions at interfaces [38, 39, 40], they are often limited by computational cost or model dependencies. Continuum models based on dielectric theory [41], such as those by Levin et al. [42], offer an efficient and insightful alternative [43, 44, 45]. These models suggest that cavity formation energies and dielectric response can drive adsorption or exclusion at interfaces.

In this work, we extend this continuum perspective by studying the Casimir–Polder interaction between a solvated particle, such as atoms, molecules and nanoparticles, and a planar wall in the polarisable continuum model (PCM) framework, deriving the perturbation of the interaction when the particle is in close proximity to the wall. Within PCM, the particle is embedded in a vacuum-like cavity surrounded by a dielectric medium [46]. We focus on the regime

where the particle–wall distance becomes smaller than the cavity radius, such that the vacuum cavity opens toward the wall. This geometric configuration leads to a partial exposure of the particle's vacuum environment to the surface, modifying the local field response and dispersion interaction. We show that this opening alters the Casimir–Polder potential in nontrivial ways and may allow for novel control over dispersion-mediated forces in solution.

2 Modelling

The dispersion interaction between a neutral, polarisable particle at position \mathbf{r}_A with polarisability $\alpha(\omega)$ and a macroscopic body at temperature T is determined by the Casimir–Polder interaction [18]

$$U_{\text{CP}}(\mathbf{r}_A) = \mu_0 k_B T \sum_{n=0}^{\infty} {}' \xi_n^2 \text{Tr} [\alpha(i\xi_n) \cdot \mathbf{G}(\mathbf{r}_A, \mathbf{r}_A, i\xi_n)] , \quad (1)$$

with the vacuum permeability μ_0 and the Boltzmann constant k_B . This interaction can be understood as an exchange of virtual photons, described by the Matsubara frequencies $\hbar\xi_n = 2\pi n k_B T$, where \hbar is the reduced Planck constant. The scattering Green function $\mathbf{G}(\mathbf{r}_A, \mathbf{r}_A, i\xi)$ describes the back-scattering of a virtual photon created at the position \mathbf{r}_A with frequency $i\xi$, caused by the ground-state fluctuations of the electromagnetic fields from the surrounding objects. The primed sum in Eq. (1) means that the $n = 0$ term of the sum is weighted by a factor $1/2$,

$$\sum_{n=0}^{\infty} {}' a_n = \frac{1}{2} a_0 + \sum_{n=1}^{\infty} a_n . \quad (2)$$

2.1 Solvent effects

We consider the typical case of a particle in a liquid with dielectric function $\varepsilon_L(\omega)$ located in front of a dielectric planar surface with dielectric function $\varepsilon_S(\omega)$, leading to the well-known potential C_3 representation of the Casimir–Polder potential,

$$U_{\text{CP}}(\mathbf{r}_A) = -\frac{C_3}{z_A^3} . \quad (3)$$

This potential is derived from the scattering Green function for a planar two-layer system [46]

$$\mathbf{G}(\mathbf{r}_A, \mathbf{r}_A, \omega) = \frac{c^2}{32\pi\varepsilon_L(\omega)\omega^2 z_A^3} \frac{\varepsilon_S(\omega) - \varepsilon_L(\omega)}{\varepsilon_S(\omega) + \varepsilon_L(\omega)} \begin{pmatrix} 1 & 0 & 0 \\ 0 & 1 & 0 \\ 0 & 0 & 2 \end{pmatrix} , \quad (4)$$

with the speed of light c . Inserting the planar Green function (4) into the Casimir–Polder formulation of (1) determines the dispersion coefficient C_3 ,

$$C_3 = \frac{k_B T}{8\pi\varepsilon_0} \sum_{n=0}^{\infty} {}' \frac{\alpha(i\xi_n)}{\varepsilon_L(i\xi)} \frac{\varepsilon_S(\omega) - \varepsilon_L(\omega)}{\varepsilon_S(\omega) + \varepsilon_L(\omega)} , \quad (5)$$

with vacuum permittivity $\varepsilon_0 = (\mu_0 c^2)^{-1}$. It can be seen that the permittivity of the surrounding medium screens the medium-assisted C_3 coefficient $\varepsilon_L(i\xi)$ compared to the same situation in vacuum ($\varepsilon_L(i\xi) = 1$). Due to the electrodynamical (frequency-dependent) screening, the van der Waals interaction between two particles in water is effectively suppressed by a factor of two. In contrast, the Coulomb force is suppressed by a factor of 80. [43]

Beyond the screening impact of the surrounding media, a further effect occurs, which is related to the Pauli repulsion between the atom and the solvent, leading to an exclusion volume V_C around the dissolved particle. This exclusion volume means there is a vacuum layer between the particle and the solvent. Thus, the scattered virtual photon has to pass this interface by mediating the interaction. The effect is usually considered via the excess or effective polarisability models, [46] which modifies the polarisabilities to include local-field corrections for the photon propagation. The simplest model considers a point-like particle in the centre of a spherical vacuum cavity with radius $R_C = \sqrt[3]{3V_C/(4\pi)}$ known as Onsager's real cavity model [46, 47]

$$\alpha(i\xi) \mapsto \left(\frac{3\varepsilon_L(i\xi)}{1 + 2\varepsilon_L(i\xi)} \right)^2 \alpha(i\xi) , \quad (6)$$

which is the square of the zeroth order Mie transmission coefficient, which includes the inwards and outwards propagation of the photon through the interface. However, this model is restricted to the scenario that the same media surrounds the particle in all directions.

2.2 The open cavity

Onsager's real cavity model, introduced in the previous section, is restricted to particles homogeneously surrounded by a medium. This model will fail when the particle approaches a solid surface where the medium will be displaced. We applied the Born series expansion for the scattering Green function to model this scenario. [18, 48] This approach separates the scattering processes according to the number of scattering events. Its first order reads [49]

$$\mathbf{G}(\mathbf{r}_A, \mathbf{r}_A, \omega) = \frac{\omega^2}{c^2} \int_{\mathbb{R}^3} \frac{d^3 s \chi(\mathbf{s}, \omega)}{1 + \chi(\mathbf{s}, \omega)/3} \mathbf{R}(\mathbf{r}_A, \mathbf{s}, \omega) \cdot \mathbf{R}(\mathbf{s}, \mathbf{r}_A, \omega), \quad (7)$$

with the spatially-dependent susceptibility of the surrounding media $\chi(\mathbf{s}, \omega) = \varepsilon(\mathbf{s}, \omega) - 1$ and the regular part of the free-space Green function [49]

$$\mathbf{R}(\mathbf{r}, \mathbf{r}', \omega) = \frac{q}{4\pi} \left[f\left(\frac{1}{q\varrho}\right) \mathbb{I} - g\left(\frac{1}{q\varrho}\right) \frac{\boldsymbol{\varrho} \otimes \boldsymbol{\varrho}}{\varrho^2} \right] e^{iq\varrho}, \quad (8)$$

with the three-dimensional unit matrix \mathbb{I} , the relative coordinate $\boldsymbol{\varrho} = \mathbf{r} - \mathbf{r}'$, its absolute value $\varrho = |\boldsymbol{\varrho}|$, absolute value of the wave vector $q = \omega/c$ and the functions $f(x) = x + ix^2 - x^3$ and $g(x) = x + 3ix^2 - 3x^3$. By assuming the particle-surface separations d to be smaller than the wavelength of the dominant atomic transition, $d \ll \omega_{\max}/c$, the non-retarded limit can be applied to lead to

$$\text{Tr} [\mathbf{R}(\mathbf{r}, \mathbf{s}, i\xi) \cdot \mathbf{R}(\mathbf{s}, \mathbf{r}, i\xi)] = \frac{3c^4}{8\pi^2 \xi^4 \varrho^6}. \quad (9)$$

Thus, to first order, the Casimir–Polder potential within an arbitrary environment can be written via the Hamaker approach [50]

$$U_{\text{CP}}(\mathbf{r}_A) = -\frac{9k_B T}{8\pi^2 \varepsilon_0} \sum_{n=0}^{\infty} {}' \alpha(i\xi_n) \int_{\mathbb{R}^3} d^3 s \frac{\varepsilon(\mathbf{s}, \omega) - 1}{\varepsilon(\mathbf{s}, \omega) + 2} \frac{1}{|\mathbf{r}_A - \mathbf{s}|^6}, \quad (10)$$

summing (integrating) the pairwise interactions between a particle at position \mathbf{r}_A and a volume element at position \mathbf{s} . Hence, the Casimir–Polder interaction is determined by the summation (integration) of van-der-Waals interactions. This model is convenient to introduce the geometry of a system beyond the well-known analytical systems (planar, cylindrical, and spherical multilayered systems) [18, 48] by considering weakly responding materials. In Eq. (10), the Mie reflection coefficient, $(\varepsilon - 1)/(\varepsilon + 2)$, can be seen, which will generate a deviation from the well-known Casimir–Polder scenario in front of an infinite half-plane, which requires the Fresnel-coefficient, $(\varepsilon - 1)/(\varepsilon + 1)$. Thus, to ensure reproducing the correct limit for a planar interface, this Hamaker approach needs to be renormalised, in analogy to Ref. [15, 6], and thus the Casimir–Polder interaction reads

$$U_{\text{CP}}(\mathbf{r}_A) = -\frac{6}{\pi} \int d^3 s \frac{C_3(\mathbf{s})}{|\mathbf{r}_A - \mathbf{s}|^6}, \quad (11)$$

with the C_3 -coefficient of the volume element at position \mathbf{s}

$$C_3(\mathbf{s}) = \frac{k_B T}{8\pi \varepsilon_0} \sum_{n=0}^{\infty} {}' \alpha(i\xi_n) \frac{\varepsilon(\mathbf{s}, i\xi_n) - 1}{\varepsilon(\mathbf{s}, i\xi_n) + 1}. \quad (12)$$

To apply the generalised Hamaker approach (11) to the open cavity, the integration volumes need to be specified. Following the point-particle assumption, the resulting cavities have spherical shapes with the molecule's cavity radius R_1 and the radius of the occupation volume of a solvent molecule R_2 . The resulting geometric arrangement of the solvent around the molecule will be rotationally symmetric according to the surface's normal as depicted in Fig. 1. The particle is located in the vacuum bubble (white area) with vanishing contrast; thus, the remaining volume integral has to be considered with respect to the solid surface (hatched area) and the surrounding liquid material (grey area), following the scenario described by Duignan et al.[44]. Transforming the integral (11) into cylindrical coordinates ($d^3 s = \varrho d\varrho d\varphi dz$), the angular integral can be ruled out, and the radial boundary between the vacuum and liquid phase can be described by

$$R(\tau; z) = \begin{cases} \sqrt{R_1^2 - \tau^2}, & \text{if } \tau < z_b, \\ x_2 - \sqrt{R_2^2 - (\tau - z_2)^2} & \text{if } z_b \leq \tau \leq z, \end{cases} \quad (13)$$

with the boundary point $z_b = R_1(z - R_2)/(R_1 + R_2)$. The total geometry is described by both radii R_1 and R_2 and the molecule-surface-distance. Via the angle of the boundary point, $\cos \alpha = z_b/R_1$, the central point of the solvent's occupation volume can be derived $(z_2, x_2) = (R_1 + R_2)(\cos \alpha, \sin \alpha)$.

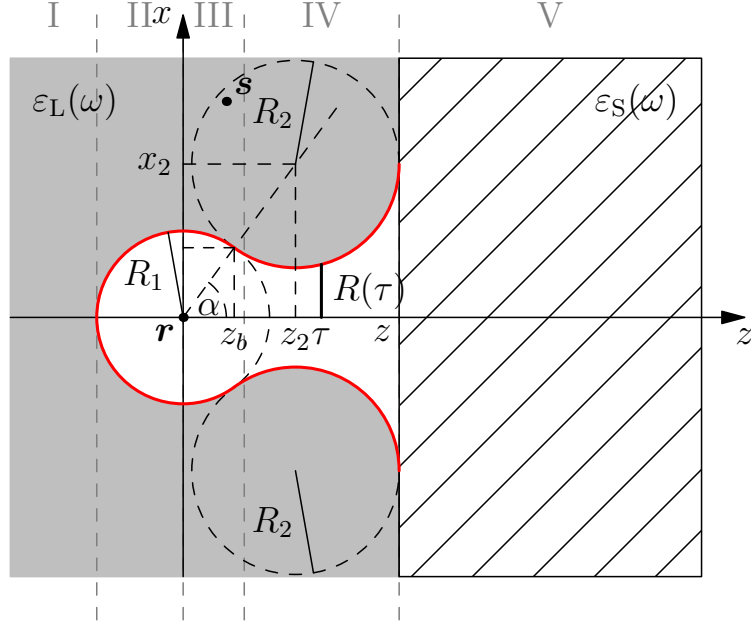


Figure 1: Cross-section through the considered system: a point-particle located at \mathbf{r} embedded in a medium (grey area) with dielectric function $\varepsilon_L(\omega)$ creates a vacuum bubble with radius R_1 surrounding it. Close to a dielectric interface $\varepsilon_S(\omega)$ (hatched area) at a distance z , the particle will displace the surrounding media and open the cavity. The single medium particles occupy a spherical volume with a radius R_2 , leading to the opened cavity illustrated in white, bounded by a profile (red line). To describe the profile mathematically, the centre of the circle of the medium particles is labelled with the coordinates (z_2, x_2) , and the touching points are in the plane $z = z_b$. The three-dimensional scenario is a body of rotation around the z -axis. To describe the Casimir–Polder interaction between the particle and the surrounding material, the van der Waals interaction must be integrated over the entire volume, split into five regions I–V.

To estimate the Casimir–Polder potential for this system according to Eq. (11), the van der Waals interaction has to be integrated over the entire space, which reduces in the considered scenario to the integral over the hatched and grey areas in Fig. 1. Due to the linearity of the integral, the Casimir–Polder potential can be split into contributions from five regions, marked in Fig. 1 with Roman numbering,

$$U_{\text{CP}}^{\text{OC}}(z) = U_{\text{CP}}^{\text{I+II}} + U_{\text{CP}}^{\text{III}}(z) + U_{\text{CP}}^{\text{IV}}(z) + U_{\text{CP}}^{\text{V}}(z). \quad (14)$$

The first two regions provide constant energy because they are independent of the separation between the particle and the interface, determined only by the cavity radius R_1 ,

$$U_{\text{CP}}^{\text{I+II}} = -\frac{4C_3^{\text{L}}}{R_1^3}. \quad (15)$$

In the third region, the Casimir–Polder potential reads

$$U_{\text{CP}}^{\text{III}}(z) = -\frac{3C_3^{\text{L}}}{R_1^3} \frac{z - R_2}{R_1 + R_2}. \quad (16)$$

In the cavity-opening region IV, the potential reads

$$U_{\text{CP}}^{\text{IV}}(z) = -\frac{12C_3^{\text{L}}R_2}{\pi R_1^3 (R_1 + 2R_2)^3} \frac{\Lambda_{\text{N}}}{\Lambda_{\text{D}}}, \quad (17)$$

with

$$\begin{aligned} \Lambda_{\text{N}} = & 8R_2^7\tilde{h} + 64R_2^6\tilde{h} \left(R_1 + \frac{3}{8}h_3 + \frac{z}{2} \right) + R_2^5 \left\{ 12R_1^2 \left(9\tilde{h} - 1 \right) + 4R_1 \left[h_3 \left(14\tilde{h} - 1 \right) - 3z \right] \right. \\ & \left. - 16\tilde{h}z \left(h_3 + 3z \right) \right\} + R_2^4 \left\{ 2R_1^3 \left(50\tilde{h} - 11 \right) + R_1^2 \left[64h_3 \left(\tilde{h} - \frac{5}{32} \right) - 2z \left(16\tilde{h} - 7 \right) \right] \right\} \end{aligned}$$

$$\begin{aligned}
 & -32zR_1 \left[z \left(\frac{3}{2}\tilde{h} - \frac{1}{4} \right) + h_3\tilde{h} \right] + 16\tilde{h}z^3 \} + 58R_1R_2^3 \left\{ R_1^3 \left(\tilde{h} - \frac{9}{29} \right) \right. \\
 & \left. + R_1^2 \left[-\frac{z}{29} (16\tilde{h} + 3) + \frac{20}{29}h_3 \left(\tilde{h} - \frac{1}{5} \right) \right] - \frac{16}{29}R_1z \left[z \left(\frac{3}{4}\tilde{h} - \frac{3}{8} \right) + h_3\tilde{h} \right] + \frac{8}{29}z^3\tilde{h} \right\} \\
 & + 24R_1^2R_2^2 \left\{ R_1^3 \left(\tilde{h} - \frac{7}{24} \right) + R_1^2 \left[\frac{7}{12}h_3 \left(\tilde{h} - \frac{1}{7} \right) - z \left(\frac{\tilde{h}}{3} - \frac{1}{24} \right) \right] - \frac{2z}{3} \left(R_1h_3\tilde{h} - \frac{z}{2} \right) + \frac{\tilde{h}z^3}{3} \right\} \\
 & + 7R_1^4R_2 \left[R_1^2 \left(\tilde{h} - \frac{1}{7} \right) + \frac{R_1}{7} \left(2h_3\tilde{h} + z \right) - \frac{4z}{7} \left(h_3\tilde{h} - \frac{z}{2} \right) \right] + R_1^7\tilde{h}, \tag{18}
 \end{aligned}$$

$$\begin{aligned}
 \Lambda_D = & 5R_1^4R_2 + 12R_1^3R_2^2 + 8R_1^2R_2^2(3R_2 - z) + 2R_2h_3 \left([R_1 + R_2]^2 + R_2^2 \right) (R_1 + 3R_2 - 2z) \\
 & + R_1^5 + 4R_1R_2^3(7R_2 - 4z) + 4R_2^2(R_2^3 + 4R_2^2z - 6R_2z^2 + 2z^3), \tag{19}
 \end{aligned}$$

$$\tan h_1 = \left\{ 2R_2(R_2 - R_1 - 2z)h_3 + \left[(R_1 + R_2)^2 + R_2^2 \right] (R_1 + z) \right\} \{R_1(R_1 + 2R_2)h_3\}^{-1}, \tag{20}$$

$$h_2 = \arctan \frac{2R_2(R_2 - z)}{R_1(R_1 + 2R_2)}, \tag{21}$$

$$h_3 = \sqrt{(R_1 + z)(R_1 + 2R_2 - z)}, \tag{22}$$

$$\tilde{h} = h_1 - h_2. \tag{23}$$

Finally, the interaction between the dissolved particle and the interface in region V

$$U_{\text{CP}}^V(z) = -\frac{C_3^S}{z^3}, \tag{24}$$

with the C_3 coefficients for the liquid (X = L) and solid (X = S)

$$C_3^X = \frac{k_B T}{8\pi\epsilon_0} \sum_{n=0}^{\infty} \alpha'(\text{i}\xi_n) \frac{\varepsilon^X(\text{i}\xi_n) - 1}{\varepsilon^X(\text{i}\xi_n) + 1}. \tag{25}$$

2.3 Corrections to the Hamaker approach

The Casimir–Polder potential for the open Onsager cavity (14) is based on the Hamaker approach (7), as the pairwise summation of the interaction. Thus, it captures only the leading order of the interaction [15, 6]. The Onsager's real cavity model considers a point particle embedded in a vacuum bubble, leading to the Casimir–Polder potential of the well-known r^{-3} form, where the polarisability of the particle has to be replaced by the excess polarisability (6). This model requires a closed cavity surrounding the particle. The model, introduced in Sec. 2.2, for the open cavity closes at distance $z_C = \sqrt{R_1(R_1 - 2R_2)} + R_2$, meaning that the validity of the model is restricted to particle-surface separations below this threshold, $z < z_C$. However, for larger separations, the potential should continuously transition into the long-range Casimir–Polder potential. Thus, the potential can be written as

$$U_{\text{CP}}(z) = \begin{cases} \lambda U_{\text{CP}}^{\text{OC}}(z), & \text{for } z < z_C \\ -\frac{C_3^S}{z^3}, & \text{for } z \geq z_C \end{cases}, \tag{26}$$

where the introduced scaling constant λ ensures the potential's continuity and corrects the pairwise summation approximation.

3 Numerical Examples

In this section, we illustrate the general theory derived above using four representative molecular–liquid–surface combinations. We consider O₂ and N₂ molecules dissolved in either water or propanol interacting with a planar polytetrafluoroethylene (PTFE) interface. These systems span a broad range of dielectric responses—from strongly polar water to weakly polar propanol—and therefore constitute suitable test cases for examining the sensitivity of the Onsager real-cavity model to the surrounding medium.

Figure 2 shows the relevant susceptibilities $\chi(i\xi) = \varepsilon(i\xi) - 1$ for water, propanol, and PTFE, together with the normalised molecular susceptibilities $\alpha(i\xi)/(4\pi\epsilon_0 V)$ of O₂ and N₂. The data are taken from Refs. [51, 28, 46]. These

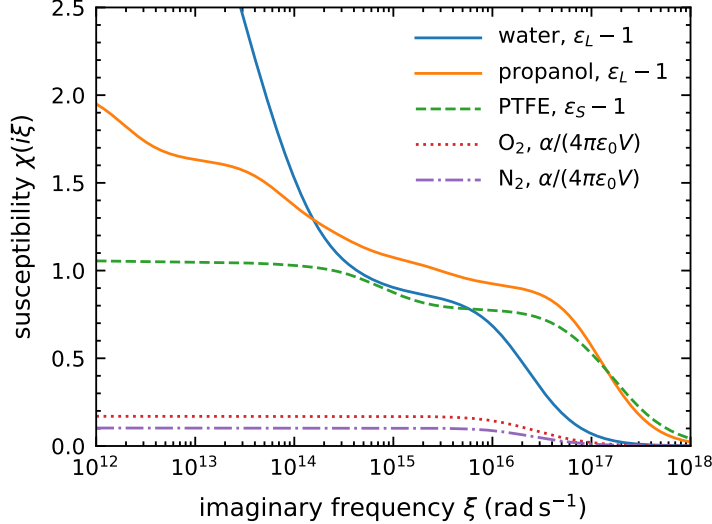


Figure 2: Dielectric function of water (solid blue line) from Ref. [51], propanol (solid orange line) and polytetrafluoroethylene (PTFE) (dashed green line) from Ref. [28] and the normalised polarisabilities for oxygen (dotted red line) and nitrogen (dash-dotted purple line) from Ref. [46].

spectral functions enter the Casimir–Polder interaction solely through the frequency-dependent material response, and thus Fig. 2 provides direct insight into the relative weight of Matsubara frequencies contributing to the dispersion interaction.

From these susceptibilities we compute the medium-assisted coefficients C_3^{med} , the liquid-screened coefficients C_3^L , and the vacuum–surface coefficients C_3^S according to Eqs. (25) and (3). The resulting values are summarised in Table 1. As expected, the strong permittivity of water yields significantly larger medium-assisted coefficients than propanol, while the differences between O_2 and N_2 reflect primarily their molecular volumes and polarisability spectra.

	Water $R_2 = 1.68 \text{ \AA}$	Propanol $R_2 = 3.497$	PTFE
O_2	$C_3 = 0.565$ $\tilde{C}_3 = 0.406$	$C_3 = 1.085$ $\tilde{C}_3 = 0.081$	$C_3 = 0.983$
N_2	$C_3 = 0.428$ $\tilde{C}_3 = 0.294$	$C_3 = 0.806$ $\tilde{C}_3 = 0.061$	$C_3 = 0.730$

Table 1: Overview of the C_3 -coefficients ($\text{meV}(\text{nm})^3$) in free-space C_3 , Eq. (25), and medium-assisted \tilde{C}_3 , Eq. (3), for the material combinations: oxygen and nitrogen molecules dissolved in water and propanol in front of a PTFE interface with the considered cavity radii R_1 and van der Waals radii R_2 . The polarisability data and cavity radii are taken from Ref. [46], the dielectric function of water from Ref. [51] and of propanol and PTFE from Ref. [28], and the van der Waals radii from Ref. [52] via the van der Waals constant b , $R_2 = \sqrt[3]{3b/4\pi N_A}$ with the Avogadro constant N_A .

Figure 3 presents the Casimir–Polder potentials for all four molecule–liquid–surface combinations considered in this work. Each panel displays the individual geometric contributions arising from the five regions of the opened Onsager cavity, as derived above, together with their corrected sum and the asymptotic medium-assisted potential $-\tilde{C}_3/z^3$. The vertical dotted line marks the characteristic distance z_C , beyond which the cavity closes and the interaction follows its far-field behaviour.

Across most of the parameter range, Region V, the solid surface, provides the dominant near-field contribution. This term corresponds to the direct, unscreened interaction between the molecule and the surface once the cavity opening points toward the interface. However, for molecules dissolved in propanol a notable modification occurs at extremely small particle–surface separations, typically $z \lesssim 10^{-2} \text{ nm}$: because the local-field correction is much weaker in propanol than in water, the geometric prefactors entering Region III become comparatively enhanced and overtake Region V in this ultrashort-distance regime. This crossover is clearly visible in the corresponding panels of Fig. 3. Outside this very small range, Region V again dominates for all systems.

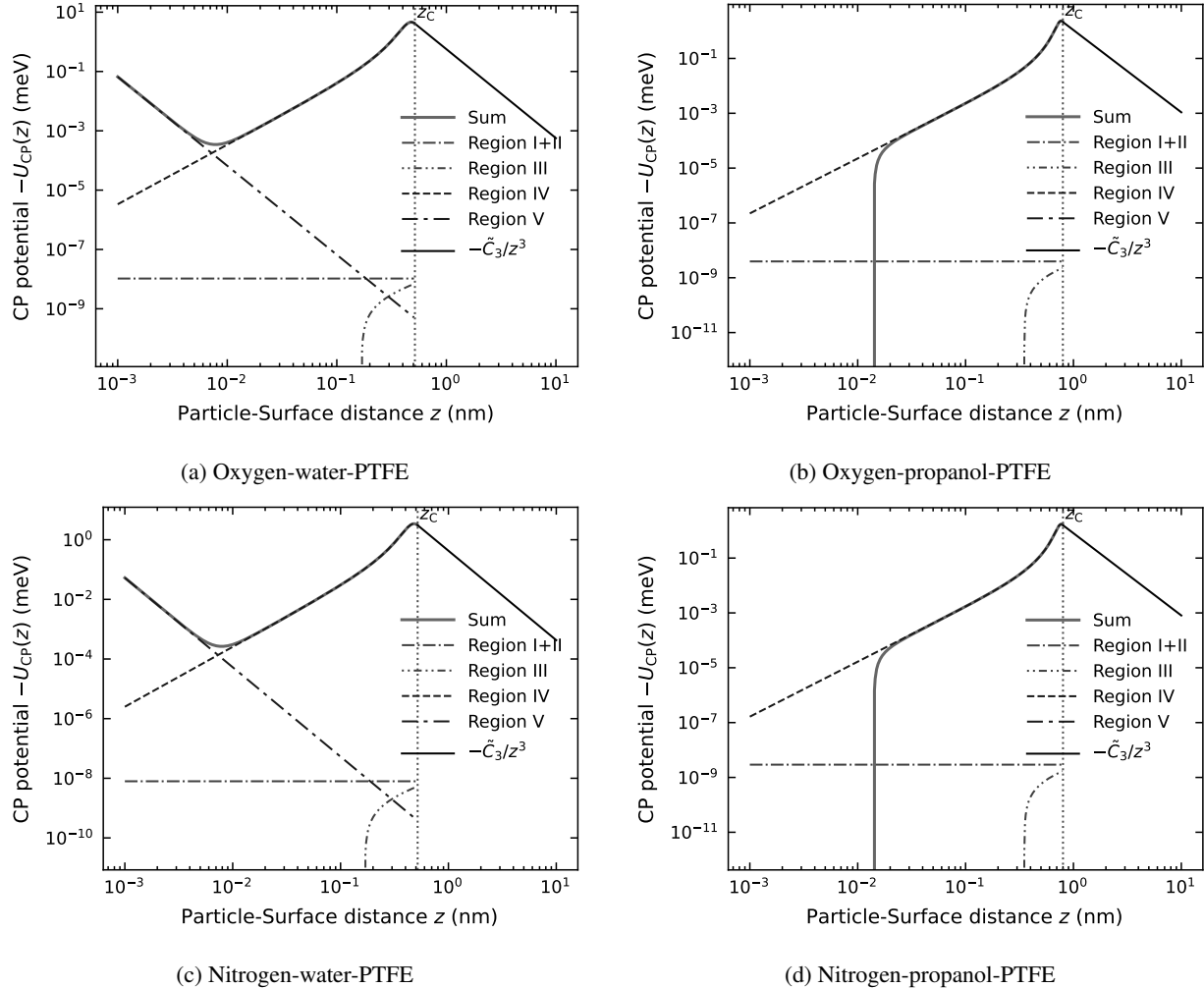


Figure 3: Casimir–Polder potential between a dissolved oxygen or nitrogen molecule near a PTFE surface. The impact of the potentials within the regions I+II (dash-dotted lines) and III (dash-double-dotted lines) is negligible in water, whereas the contribution from region III dominates potential very short separations in propanol. The dominant parts region IV (dashed lines) and V (long dashed-dotted lines) dominate the total potential (solid grey lines). Particle-surface separations, leading to a closing of the cavity, $z \geq z_C$ (vertical dotted lines) continue into the medium-assisted Casimir–Polder potential (solid black lines).

The effect of the liquid becomes apparent in the magnitude and curvature of the total potential. Water, owing to its large static permittivity, provides strong local-field screening inside the cavity, which reduces the effective coupling between the molecule and the surface. As a result, the total potential for O_2 and N_2 in water is systematically smaller than in propanol at short and intermediate distances, despite identical surface and geometric parameters. Conversely, propanol, with its much weaker dielectric response, leads to larger C_3^L and therefore to stronger potentials in the near and intermediate regimes.

For both liquids, oxygen exhibits a slightly stronger interaction than nitrogen. This difference originates primarily from the molecular polarisability spectra (see Fig. 2) and the associated cavity radii R_1 , which determine the relative weight of the higher Matsubara frequencies contributing to the interaction. At large separations $z \gg z_C$, all systems converge to a clean $-\tilde{C}_3/z^3$ power law governed solely by the medium-assisted coefficient \tilde{C}_3 of the respective liquid. The smooth matching between the scaled cavity contributions and the asymptotic curve confirms the consistency of the cavity-opening model and the scaling procedure used at z_C .

Overall, the four examples demonstrate that the interplay between the cavity geometry, the dielectric response of the host medium, and the molecular polarisability defines the detailed shape of the Casimir–Polder interaction. While the

qualitative structure of the potential is universal, the quantitative differences, in particular between water and propanol, highlight the important role of local-field effects and molecular size in nanoscale dispersion forces.

4 Conclusions

We have developed and applied an extended Onsager real-cavity approach for the Casimir–Polder interaction of small molecules dissolved in dielectric liquids near planar interfaces. Starting from a full geometric decomposition of the cavity opening, we derived analytic expressions for the five distinct regions contributing to the interaction and demonstrated how they connect smoothly to the asymptotic medium-assisted power law at large particle–surface separations. Using experimentally established dielectric response functions for water, propanol, and PTFE, together with accurate molecular polarisabilities for O₂ and N₂, we evaluated the complete distance-dependent potential for several representative systems. The resulting interaction combines strong local-field screening inside the cavity with geometry-dependent enhancements near the interface, leading to distinct near-field behaviour for different liquids and molecules. The model consistently reproduces the expected $-C_3/z^3$ asymptotics and reveals in detail how cavity-opening geometry modifies the potential at short distances.

Despite its predictive power and conceptual transparency, the present framework inherits several limitations that suggest directions for future improvements. First, the molecule is treated as a point-like particle characterised solely by its dipole polarisability. At the ultrashort distances, where parts of the cavity become comparable to molecular dimensions, higher multipole contributions and the finite size of the electron cloud may lead to quantitative deviations. Second, the model captures only attractive dispersion forces. Since the formalism does not include frequency-dependent sign changes in the reflection coefficients of the surrounding media, it cannot describe repulsive Casimir–Polder forces that arise in systems with tailored dielectric contrast or in non-equilibrium situations. Third, the dipole approximation implicit in the Onsager picture becomes questionable at the smallest distances considered, where electronic overlap, chemical forces, and short-range exchange interactions may compete with the dispersion interaction.

Addressing these limitations will require a more complete microscopic model of the cavity region, including finite-size and multipole corrections, dielectric environments that allow for sign reversals of the interaction, and a seamless coupling between dispersion and short-range chemical forces. Nevertheless, the present theory provides a consistent and quantitatively transparent baseline for understanding how local-field effects, molecular polarisability, and cavity geometry jointly shape Casimir–Polder interactions in liquids.

References

- [1] F London. The general theory of molecular forces. *J. Chem. Soc. Faraday Trans*, 33(8):8b, 1937.
- [2] Johannes Diderik van der Waals. *Over de Continuiteit van den Gas- en Vloeistofoestand [On the continuity of the gas and liquid state]*. Ph.d. thesis, University of Leiden, 1873.
- [3] F. London. Zur Theorie und Systematik der Molekularkräfte. *Z. Phys.*, 63(3-4):245–279, mar 1930.
- [4] Kellar Autumn, Yiching A Liang, S Tonia Hsieh, Wolfgang Zesch, Wai Pang Chan, Thomas W Kenny, Ronald Fearing, and Robert J Full. Adhesive force of a single gecko foot-hair. *Nature*, 405(6787):681–685, 2000.
- [5] Frank W DelRio, Maarten P de Boer, James A Knapp, E David Reedy, Peggy J Clews, and Martin L Dunn. The role of van der Waals forces in adhesion of micromachined surfaces. *Nature Mat.*, 4(8):629–634, 2005.
- [6] Johannes Fiedler and Bodil Holst. An atom passing through a hole in a dielectric membrane: impact of dispersion forces on mask-based matter-wave lithography. *Journal of Physics B: Atomic, Molecular and Optical Physics*, 55(2):025401, feb 2022.
- [7] Sapida Akhundzada, Xiaohui Yang, Johannes Fiedler, Eireen Käkel, Basim Al-Qargholi, Stefan Buhmann, Arno Ehresmann, and Hartmut Hillmer. A novel approach to construct self-assembled 3d mems arrays. *Microsystem Technologies*, 28:2139–2148, 2022.
- [8] Johannes Fiedler, Adriá Salvador Palau, Eivind Kristen Osestad, Pekka Parviainen, and Bodil Holst. Realistic mask generation for matter-wave lithography via machine learning. *Machine Learning: Science and Technology*, 4(2):025028, jun 2023.
- [9] Johannes Fiedler and Bodil Holst. A continuous beam monochromator for matter waves. *The European Physical Journal D*, 78:39, 2024.
- [10] Johannes Fiedler, Clas Persson, and Stefan Yoshi Buhmann. Spectroscopy of nanoparticles without light. *Phys. Rev. Appl.*, 13:014025, Jan 2020.

- [11] Eivind Kristen Osestad, Pekka Parviainen, and Johannes Fiedler. A novel gas sensing principle based on quantum fluctuations. *EPJ Quantum Technology*, 12:37, 2025.
- [12] R. E. Grisenti, W. Schöllkopf, J. P. Toennies, G. C. Hegerfeldt, and T. Köhler. Determination of Atom-Surface Van der Waals Potentials from Transmission-Grating Diffraction Intensities. *Phys. Rev. Lett.*, 83:1755–1758, 1999.
- [13] M. Arndt, O. Nairz, J. Vos-Andreae, C. Keller, G. van der Zouw, and A. Zeilinger. Wave-particle duality of C60 molecules. *Nature*, 401(6754):680–682, 1999.
- [14] T. Juffmann, A. Milic, M. Müllneritsch, P. Asenbaum, A. Tsukernik, J. Tüxen, M. Mayor, O. Cheshnovsky, and M. Arndt. Real-time single-molecule imaging of quantum interference. *Nature Nanotechn.*, 7:297 – 300, 2012.
- [15] Christian Brand, Johannes Fiedler, Thomas Juffmann, Michele Sclafani, Christian Knobloch, Stefan Scheel, Yigal Lilach, Ori Cheshnovsky, and Markus Arndt. A green's function approach to modeling molecular diffraction in the limit of ultra-thin gratings. *Annalen der Physik*, 527(9-10):580–591, 2015.
- [16] H. B. G. Casimir and D. Polder. The influence of retardation on the london-van der waals forces. *Phys. Rev.*, 73:360–372, Feb 1948.
- [17] I. E. Dzyaloshinskii, E. M. Lifshitz, and Lev P. Pitaevskii. General theory of van der waals' forces. *Soviet Physics Uspekhi*, 4(2):153, 1961.
- [18] Stefan Scheel and Stefan Yoshi Buhmann. Macroscopic QED - concepts and applications. *Acta Physica Slovaca*, 58(5):675–809, feb 2008.
- [19] S. Y. Buhmann. *Dispersion Forces I: Macroscopic quantum electrodynamics and ground-state Casimir, Casimir-Polder and van der Waals forces*. Springer, Heidelberg, 2012.
- [20] J. Fiedler, K. Berland, J. W. Borchert, R. W. Corkery, A. Eisfeld, D. Gelbwaser-Klimovsky, M. M. Greve, B. Holst, K. Jacobs, M. Krüger, D. F. Parsons, C. Persson, M. Presselt, T. Reisinger, S. Scheel, F. Stienkemeier, M. Tømterud, M. Walter, R. T. Weitz, and J. Zalieckas. Perspectives on weak interactions in complex materials at different length scales. *Phys. Chem. Chem. Phys.*, 25:2671–2705, 2023.
- [21] H. B. G. Casimir. On the attraction between two perfectly conducting plates. *Proc. K. Ned. Akad. Wet.*, 51:793, 1948.
- [22] A. D. McLachlan. Retarded dispersion forces between molecules. *Proc. R. Soc. A.*, 271(1346):387–401, 1963.
- [23] Peter W. Milonni. Chapter 7 - casimir and van der waals forces: Prelude. In Peter W. Milonni, editor, *The Quantum Vacuum*, pages 217 – 252. Academic Press, San Diego, 1994.
- [24] D. S. Ether, L. B. Pires, S. Umrath, D. Martinez, Y. Ayala, B. Pontes, G. R. de S. Araújo, S. Frases, G.-L. Ingold, F. S. S. Rosa, N. B. Viana, H. M. Nussenzveig, and P. A. Maia Neto. Probing the Casimir force with optical tweezers. *EPL (Europhysics Letters)*, 112(4):44001, nov 2015.
- [25] Peter Loskill, Hendrik Hähl, Thomas Faidt, Samuel Grandthyll, Frank Müller, and Karin Jacobs. Is adhesion superficial? Silicon wafers as a model system to study van der Waals interactions. *Advances in Colloid and Interface Science*, 179–182:107 – 113, 2012.
- [26] Stefan Yoshi Buhmann, Stefan Scheel, and James Babington. Universal Scaling Laws for Dispersion Interactions. *Phys. Rev. Lett.*, 104:070404, Feb 2010.
- [27] Rico F. Tabor, Rogerio Manica, Derek Y. C. Chan, Franz Grieser, and Raymond R. Dagastine. Repulsive van der Waals Forces in Soft Matter: Why Bubbles Do Not Stick to Walls. *Phys. Rev. Lett.*, 106:064501, Feb 2011.
- [28] P. J. van Zwol and G. Palasantzas. Repulsive casimir forces between solid materials with high-refractive-index intervening liquids. *Phys. Rev. A*, 81:062502, Jun 2010.
- [29] Johannes Fiedler, Kristian Berland, Fabian Spallek, Iver Brevik, Clas Persson, Stefan Yoshi Buhmann, and Mathias Boström. Nontrivial retardation effects in dispersion forces: From anomalous distance dependence to novel traps. *Phys. Rev. B*, 101:235424, Jun 2020.
- [30] Rongkuo Zhao, Lin Li, Sui Yang, Wei Bao, Yang Xia, Paul Ashby, Yuan Wang, and Xiang Zhang. Stable Casimir equilibria and quantum trapping. *Science*, 364(6444):984–987, 2019.
- [31] Maofeng Dou, Fei Lou, Mathias Boström, Iver Brevik, and Clas Persson. Casimir quantum levitation tuned by means of material properties and geometries. *Phys. Rev. B*, 89:201407, May 2014.
- [32] P. Thiyam, J. Fiedler, S. Y. Buhmann, C. Persson, I. Brevik, M. Boström, and D. F. Parsons. Ice Particles Sink below the Water Surface Due to a Balance of Salt, van der Waals, and Buoyancy Forces. *The Journal of Physical Chemistry C*, 122(27):15311–15317, 2018.

- [33] Mathias Boström, Maofeng Dou, Oleksandr I. Malyi, Prachi Parashar, Drew F. Parsons, Iver Brevik, and Clas Persson. Fluid-sensitive nanoscale switching with quantum levitation controlled by α -Sn/ β -Sn phase transition. *Phys. Rev. B*, 97:125421, Mar 2018.
- [34] Pavel Jungwirth and Douglas J. Tobias. Molecular structure of salt solutions: A new view of the interface with implications for heterogeneous atmospheric chemistry. *The Journal of Physical Chemistry B*, 105(43):10468–10472, 2001.
- [35] Pavel Jungwirth and Douglas J. Tobias. Ions at the air/water interface. *The Journal of Physical Chemistry B*, 106(25):6361–6373, 2002.
- [36] Tatsuya Ishiyama and Akihiro Morita. Molecular dynamics study of gas-liquid aqueous sodium halide interfaces. i. flexible and polarizable molecular modeling and interfacial properties. *The Journal of Physical Chemistry C*, 111(2):721–737, 2007.
- [37] Daniel J. V. A. dos Santos, Florian Müller-Plathe, and Volker C. Weiss. Consistency of ion adsorption and excess surface tension in molecular dynamics simulations of aqueous salt solutions. *The Journal of Physical Chemistry C*, 112(49):19431–19442, 2008.
- [38] Poul B. Petersen and Richard J. Saykally. On the nature of ions at the liquid water surface. *Annual Review of Physical Chemistry*, 57(Volume 57, 2006):333–364, 2006.
- [39] Pavel Jungwirth and Douglas J. Tobias. Specific ion effects at the air/water interface. *Chemical Reviews*, 106(4):1259–1281, 2006.
- [40] Yan Levin and Alexandre P dos Santos. Ions at hydrophobic interfaces. *Journal of Physics: Condensed Matter*, 26(20):203101, apr 2014.
- [41] Luca Frediani, Roberto Cammi, Stefano Corni, and Jacopo Tomasi. A polarizable continuum model for molecules at diffuse interfaces. *The Journal of Chemical Physics*, 120(8):3893–3907, 02 2004.
- [42] Yan Levin, Alexandre P. dos Santos, and Alexandre Diehl. Ions at the air-water interface: An end to a hundred-year-old mystery? *Phys. Rev. Lett.*, 103:257802, Dec 2009.
- [43] Johannes Fiedler, Michael Walter, and Stefan Yoshi Buhmann. Effective screening of medium-assisted van der waals interactions between embedded particles. *The Journal of Chemical Physics*, 154(10):104102, 2021.
- [44] Timothy T. Duignan, Drew F. Parsons, and Barry W. Ninham. Ion interactions with the air–water interface using a continuum solvent model. *The Journal of Physical Chemistry B*, 118:8700–8710, 7 2014.
- [45] Timothy T. Duignan, Drew F. Parsons, and Barry W. Ninham. Hydronium and hydroxide at the air–water interface with a continuum solvent model. *Chemical Physics Letters*, 635:1–12, 8 2015.
- [46] Johannes Fiedler, Priyadarshini Thiyam, Anurag Kurumbail, Friedrich A. Burger, Michael Walter, Clas Persson, Iver Brevik, Drew F. Parsons, Mathias Boström, and Stefan Y. Buhmann. Effective polarizability models. *The Journal of Physical Chemistry A*, 121(51):9742–9751, 2017.
- [47] Lars Onsager. Electric moments of molecules in liquids. *Journal of the American Chemical Society*, 58(8):1486–1493, 1936.
- [48] S. Y. Buhmann. *Dispersion Forces II: Many-Body Effects, Excited Atoms, Finite Temperature and Quantum Friction*. Springer Tracts in Modern Physics. Springer, Heidelberg, 2012.
- [49] Helmar Bender, Christian Stehle, Claus Zimmermann, Sebastian Slama, Johannes Fiedler, Stefan Scheel, Stefan Yoshi Buhmann, and Valery N. Marachevsky. Probing atom-surface interactions by diffraction of bose-einstein condensates. *Phys. Rev. X*, 4:011029, Feb 2014.
- [50] H.C. Hamaker. The london—van der waals attraction between spherical particles. *Physica*, 4(10):1058–1072, 1937.
- [51] Johannes Fiedler, Mathias Boström, Clas Persson, Iver Brevik, Robert Corkery, Stefan Yoshi Buhmann, and Drew F. Parsons. Full-spectrum high-resolution modeling of the dielectric function of water. *The Journal of Physical Chemistry B*, 124(15):3103–3113, 2020.
- [52] Robert C. Reid, John M. Prausnitz, and Bruce E. Poling. *The Properties of gases and liquids*. McGraw-Hill, New York, 1988.